

# Growth of boron nitride nanotubes and iron nanowires from the liquid flow of FeB nanoparticles

Kian Ping Loh <sup>a,\*</sup>, Ming Lin <sup>a</sup>, Mark Yeadon <sup>b</sup>, Chris Boothroyd <sup>b</sup>, Z. Hu <sup>c</sup>

<sup>a</sup> Department of Chemistry, National University of Singapore, Lower Kent Ridge Road, 3 Science Drive 3, Singapore 117543, Singapore

<sup>b</sup> Institute of Material Research and Engineering, 3 Research Link, Singapore 117602, Singapore

<sup>c</sup> Laboratory of Mesoscopic Materials Science and Department of Chemistry, Nanjing University, Nanjing 210093, PR China

Received 29 December 2003; in final form 28 January 2004

Published online: 21 February 2004

## Abstract

The growth of hexagonal boron nitride (BN) nanotubes and nanocages from the liquid flow of iron boride (FeB) nanoparticles has been achieved by the nitrogen plasma treatment of FeB nanoparticles at temperature close to the eutectic melting point of the alloy (<1000 °C). In addition to BN nanotubes (5–10 nm diameter), BN nanotubules (100–200 nm diameter) created by interconnected chains of BN nanocages, as well as BN hollow microspheres can be grown. The recrystallization of iron from smaller FeB particles results in crystalline iron nanowires encapsulated by BN. These observations suggest that nanostructure formation can be controlled by the liquid flow of nanoparticles where interfacial wetting behaviour and surface tension play a key mechanistic role. © 2004 Elsevier B.V. All rights reserved.

## 1. Introduction

Boron nitride (BN) nanotubes have attracted interests due to its unique properties of wide band gap, thermal stability, oxidation resistance, and a constant band gap independent of the chirality of the nanotube [1]. BN nanotubes have been synthesized by a range of methods ranging from arc deposition, laser ablation, chemical vapor deposition to solid-state ball milling methods [2–7]. Non-catalytic growth methods have also been demonstrated [8–10]. Most of these methods require thermal conditions higher than 1200 °C and the yield of BN nanomaterials is often low. Narita and Oku [11–13] researched on the arc-melting of borides such as TiB<sub>2</sub>, VB<sub>2</sub>, NbB<sub>2</sub>, LaB<sub>6</sub> for the production of BN nanocapsules and nanotubes. The formation enthalpies of BN from the respective borides were considered as the key factor in catalyst design. However another important factor is the composition of the boride phase in the design of the catalyst, since this will influence the eutectic melting point. A lower eutectic melting point will

promote the ready formation of a molten phase to initiate the vapor–liquid-phase mechanism, thus allowing the phase segregation of BN nanomaterials at lower temperatures.

The direct plasma nitridation of iron borides at a moderately low temperatures, i.e. <1000 °C, for the growth of BN nanomaterials has not been demonstrated. In this work, we carried out direct plasma nitridation of iron boride (FeB) nanoparticles in order to prepare BN nanomaterials at temperatures lower than 1000 °C. The reaction of FeB nanoparticles with nitrogen or ammonia can result in the growth of core-shell structures consisting of an inert BN coat encapsulating an iron core. The growth of such metal-encapsulated nanomaterials, where the outer sheath consists of an inert coating to prevent the oxidation of the inner metal nanoclusters, offers important technological applications in ferromagnetism and quantum devices. Interesting host-guest chemistry or supra-atom properties may be exhibited by metallo-fullerene type structure where the metal atom is inserted in the center of the BN nanosphere. Recent studies of iron nitride-encapsulated BN nanoparticles showed ferromagnetism properties [14,15].

\* Corresponding author. Fax: +65-6779-1691.

E-mail address: [chmlohkp@nus.edu.sg](mailto:chmlohkp@nus.edu.sg) (K.P. Loh).

In this work, we discover that due to the lability of the liquid particle shape, the structural morphology of the phase-segregated components is controlled by internal parameters of the iron–BN system such as surface tension of liquid iron and the wetting properties of the iron–BN interface.

## 2. Experimental

The FeB nanoparticles employed as catalyst in this experiment were prepared by ball-milling water-free FeCl<sub>3</sub> and NaBH<sub>4</sub> (1:3:3 in mole ratio) for 8 h followed by annealing in Argon at 500 °C for 3 h. For direct transmission electron microscopy (TEM) observation, the FeB catalyst was ultrasonicated in water and then dispersed on a silicon with a hole in the center. The TEM study was carried out in a JEOL JEM 2000 V UHV TEM equipped with a Gatan Image Filter and an ammonia gas dosing source. Ammonia gas was admitted to observe the in situ reaction in one study.

In another series of studies, samples were prepared by casting FeB nanoparticles onto Si (100) wafers and these were then introduced into a commercial 2.45 GHz microwave plasma chemical vapor deposition system. The sample was heated to 900 °C during plasma treatment. The gaseous precursor consisted of a mixture of N<sub>2</sub>:H<sub>2</sub> in a volumetric flow ratio of 3:1 at a pressure of 20 Torr. Following the plasma treatment, a whitish-grey product covered the sample, this was scraped off, ultrasonicated in an ethanol suspension, and then cast onto a TEM grid for observation with a Phillips 300 keV TEM.

## 3. Results and discussion

TEM observation of the FeB particles before reaction shows that the nanoparticles are approximately 10–15 nm in diameter. If the sample is heated to 900 °C, significant sintering and agglomeration of the FeB nanoparticles are observed. Grazing angle X-ray diffraction (XRD) reveals that the initial FeB phase is largely amorphous and mixed with crystalline iron, but following nitrogen plasma treatment at 900 °C, we can detect the growth of peaks assignable to Fe<sub>23</sub>B<sub>6</sub>, Fe<sub>8</sub>B,

Fe<sub>2</sub>N and FeN, as well as a small peak due to BN (002), suggesting the formation of crystalline *h*-BN.

A comprehensive analysis of the morphologies of the BN nanomaterial and the adjacent FeB particles from which it ensues indicates a relationship between the size of the FeB particle and the shape and form of its BN derivative. In actual experimental conditions, where we subject the FeB-cast silicon substrate to N<sub>2</sub>-plasma treatment, product distribution on the silicon substrate

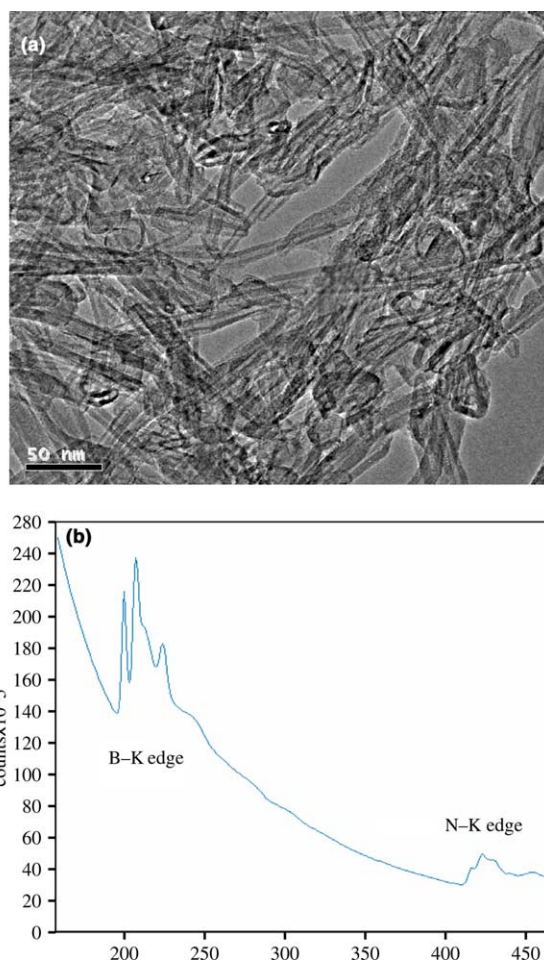


Fig. 1. (a) TEM image of high density BN ‘bamboo-like’ nanotubes recovered from the FeB nanoparticles after nitrogen-plasma treatment at 900 °C. (b) Electron energy loss spectrum collected from the BN nanomaterials in this work, showing the B 1s and N 1s K-edges, and a notable absence of carbon.

Table 1  
Relationship between the FeB particle size and the morphology of the nanomaterials ensuing from it

Size of associated FeB particle (nm)	Morphology	Length	Quantity	Reference
10	Nanotubes	200 nm	Many	Fig. 1
50–100	Nanocages and nanotubules Iron nanowires	2–3 μm 0.5–1 μm	Not so much Few	Fig. 2 Fig. 4
500	Microspheres	0.5 μm	Many	Fig. 3

is quite heterogeneous and the nanotube diameter correlation is complicated by nanoparticle-substrate interaction, mobility of particles at elevated temperatures and fragmentation and coagulation process. Underpinning this relationship is the relative ease for which the particle undergoes liquid-flow. The FeB phase diagram [16] indicates that the FeB is stable to 1650 °C. But as the B content decreases below 50 at.% at a temperature of 1000 °C, Fe<sub>2</sub>B (solid) and liquid FeB are the equilibrium phases (stable to 1389 °C), whilst below 33% B, solid Fe and liquid Fe<sub>2</sub>B are expected, with a eutectic at 1174 °C. The FeB particles we use have boron content below 33%, so liquid-like behaviour can be expected at ~1000 °C. The well-known Gibbs–Thompson effect predicts that for particles with sizes below 100 nm, the melting occurs at a significantly lower temperature compared to values in the standard phase diagram, thus fluid-like motion can be attained more readily. Table 1 summarizes the apparent relationship between the size of the FeB particle and the BN nanomaterial that ensued from it, as was observed in this work. It is more difficult for the larger particles to achieve fluid-like motion compared to smaller particles. So if the smaller FeB particles aggregate to form a FeB particle larger than 200 nm, the mobility of this particle is restricted and only an outer BN microcapsule grows on it. Nanotubules are generally observed to grow from FeB particles with sizes in the range of 100–200 nm, because

these particles melt and flow readily, and trace out nanotubules with bamboo-like segments in its motion. What is interesting are FeB particles with sizes ranging from 50 to 100 nm, smaller BN nanotubes and nanocapsules are readily created from these, and in addition, these FeB particles readily melt and recrystallize into crystalline Fe nanowires ensheathed by BN. A detailed discussion of the various structural polytypes follows below.

Generally, the most predominant products recovered from the grey deposits following the nitrogen-plasma treatment of the FeB nanoparticles are BN nanotubes, characterized by the TEM picture in Fig. 1a. These are BN bamboo-like nanotubes with diameters of 5–10 nm. The internal microstructure is characterized by closed conical segment. This arises from the periodic accumulation of BN material following the diffusion of N into the body of the FeB particle, and then periodic segregation of BN towards the particle surface, leading to the formation of periodic BN compartments. A phenomenological model explaining the growth of such structures has been proposed by Louchev recently [17]. EELS spectra recorded of all the BN nanomaterials in this work show distinct B and N *K*-edges, with notable absence of carbon. Fig. 1b shows a representative spectrum, the ionization edges  $\pi^*$  and  $\sigma^*$  correspond to the sp<sup>2</sup> hybridization of BN, as expected of the formation of hexagonal BN.

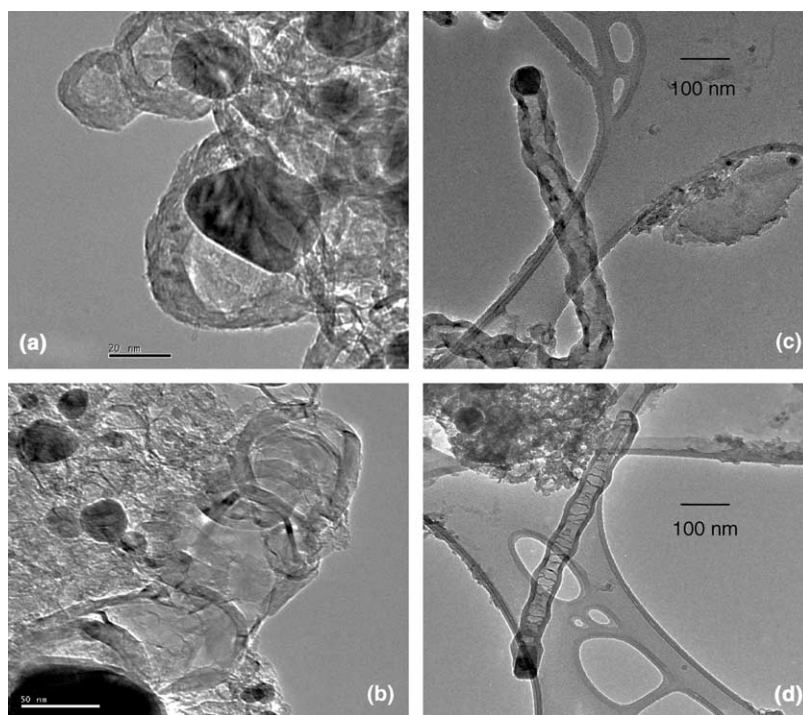


Fig. 2. TEM showing in situ formation of BN nanocages from the ammonia nitridation of the FeB particles in high vacuum: (a) BN nanocages with ejected metal encapsulates; (b) interconnected BN nanocages traced out by the liquid flow of the FeB particle; (c) and (d) are TEM images of longer BN nanotubes traced out by a single FeB particle after nitrogen plasma treatment.

For FeB particles with sizes between 50 and 100 nm, nanotubules or nanocapsules are readily formed from them. To understand the growth mechanism of the BN nanomaterials, we introduced a silicon sample with a hole in it, and which was pre-cast with FeB particles, onto the pole piece of an in situ TEM system. This allowed the direct in situ observation of the nitridation reaction with ammonia at a background pressure of  $1 \times 10^{-6}$  Torr. At 900 °C, sintering of the FeB particles, as well as the growth of BN layers on the periphery of the aggregated particles could be observed. Isolated FeB particles that escaped sintering afforded interesting observation point for the sequential growth of BN nanocages. Fig. 2a shows the TEM images of BN nanocages consisting of multi-layered hexagonal BN with some FeB particles leaving the BN nanocages. Fig. 2b traces the fluid-like profile of a FeB particle ‘in-motion’ and circumscribing four shells of interconnected BN nanocages. Our observation of the process in real time shows that the BN layers are formed at the surface of the fluid FeB particle, once a certain critical thickness of the BN external coat is attained, the FeB particle is expelled from the first BN shell and immediately within several seconds, a second layer of BN will encapsulate the FeB particle, following by its ejection, and the process repeats itself to form the third and fourth shell. The edges of these shells are interconnected because the reactive dangling bonds of the edges of the curled walls are still in contact with the FeB particle after its ejection. However we failed to observe the growth of longer BN nanotubes, and the yield of BN nanomaterials was generally low due to the lower reaction efficiency in the high vacuum reaction condition ( $1 \times 10^{-6}$  Torr).

If the FeB particles were treated with nitrogen plasma at 20 Torr pressure and 1000 °C, the reaction yield for BN nanomaterials increased considerably. In this case, we can observe for example a one-micron long nanotubule ‘traced’ out by one single FeB particle, as shown in Fig. 2c,d. It is noteworthy to point out two facts: First, the nanotubule formed is a shape-transform of the FeB particle as judged by the BN walls surrounding the *exterior* of the FeB particle. Second, the nanotubule walls are curvy and twisted-looking, and are formed by a string of interconnected BN nanocages circumscribed by the FeB particle in its liquid flow.

Based on these experimental observations, we can deduce that the growth occurs at the inner face between the BN walls and the FeB particle. Nitrogen-bearing species may be supplied to the particle:shell interface either by diffusion through the shell wall, or by diffusion along the particle:shell interface. Diffusion of N–BN layers has a high activation barrier with a characteristic time that is much larger compared to diffusion through the liquid particle. Low diameter liquefied nanoparticles are characterized by significantly shorter times of N diffusion through the particle body which is important

for BN nanotube formation by the segregation process. The dissolution of nitrogen in the molten FeB results in the formation of BN, which is insoluble and segregates as an outer BN shell. Following the segregation of a single BN shell, growth of further BN shells proceeded between the inner face of the shell and the FeB particle which is wetting it by the continuous epitaxial precipitation of BN from the molten FeB, i.e. the growth occurs between a wetted liquid-solid interface. The inward directed growth of the BN shells will result in a continuously shrinking inner volume and increasing tensional forces at the Fe–BN interface. At any aperture in the BN shell, capillary action will draw the molten FeB out from within and through it as the compressive forces build up to a critical level, and an incipient void will be left behind. The process then repeats itself as the ejected FeB particle is surrounded by another growing BN shell. Interconnections of these nano-shells result in a BN nanotubule, analogous to the images in Fig. 2b. The internal segments in the tubule in Fig. 2d are the apertures where the FeB particle squeezes out from. This mechanism is analogous to the catalytic capillarity mechanism proposed by Chadderton in their ball-mill reactions of graphite and BN where a skeletal BN

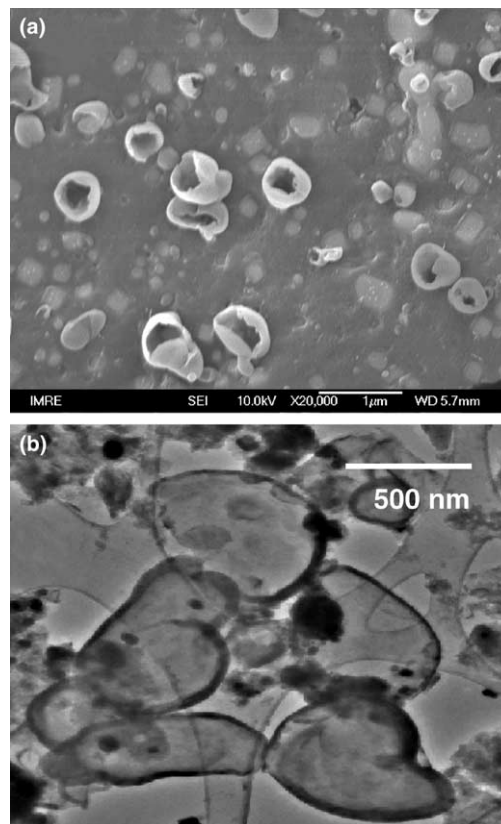


Fig. 3. (a) SEM images of the BN microcapsule which resembles cracked egg-shells, obtained after thick BN shells nucleated on the aggregated FeB particle. (b) TEM images showing thinner-walled, hollow BN capsules.

nanotube with continuous endohedral capillary structure is observed [7,18,19]. It is possible that the ball milling process creates FeB particle from Fe impurity and BN.

How strong is the compressive force for the ejection of the inner FeB particle? Evidences suggest that the compressive force is strong enough to crack thick BN microcapsules. In these experiments, the FeB particles were cast on a silicon wafer and subjected to nitrogen plasma treatment. Following the nitrogen plasma treatment and cooling, many micron-sized egg shell-like BN microcapsules were formed, as shown by the SEM images in Fig. 3a. What is noteworthy is that all the BN microcapsules have a crack in the shell. Next to these cracked BN 'egg-shells' can be found single crystal, well-faceted Fe. This suggests that molten metal drops created from the aggregation of FeB particles are contained in the micron-sized solid BN capsule during the plasma treatment and high-temperature annealing. Compressive stress created by the inward-growing BN shells caused the molten Fe to break through, escape and recrystallize into single crystals next to it, leaving behind the cracked BN egg-shells. The internal microstructure of some of the thinner, transparent BN microcapsules is shown by the TEM images in Fig. 3b. These thinner capsules be-

come disengaged from the FeB particles after ultrasonication. Such shell-like BN sub-micron and micron scale structures have also been observed in laser ablation studies by Komatsu and coworkers [20,21].

In addition to BN nanotubes and nanospheres, metallic nanoparticles with high shape anisotropy can be found among the products after the nitrogen plasma treatment. The relative ease of liquidification and capillary flow of smaller FeB particles, followed by recrystallization, results in the growth of iron nanowire encapsulated by disordered hexagonal BN sheets. Fig. 4a shows the TEM images of metallic nanoparticles entrapped in the mass of BN sheets after capillary flow. Fig. 4b shows the image of a long iron nanowire encapsulated in BN. Higher magnification images in Fig. 4c,d reveal that the interface between the BN and Fe consists of disordered *h*-BN, and crystalline *h*-BN layers nucleates on top of the disordered *h*-BN. The composition was verified by elemental mapping with EELS in Fig. 5, which confirmed that the inner filling is elemental iron, whilst the outer coating is BN. The wrap around of the entire iron wire by BN layers attests to the good wetting properties between iron and BN. Babonneau and coworkers reported the synthesis of vertically elongated nanoparticles of Fe<sub>2</sub>N encapsulated in disor-

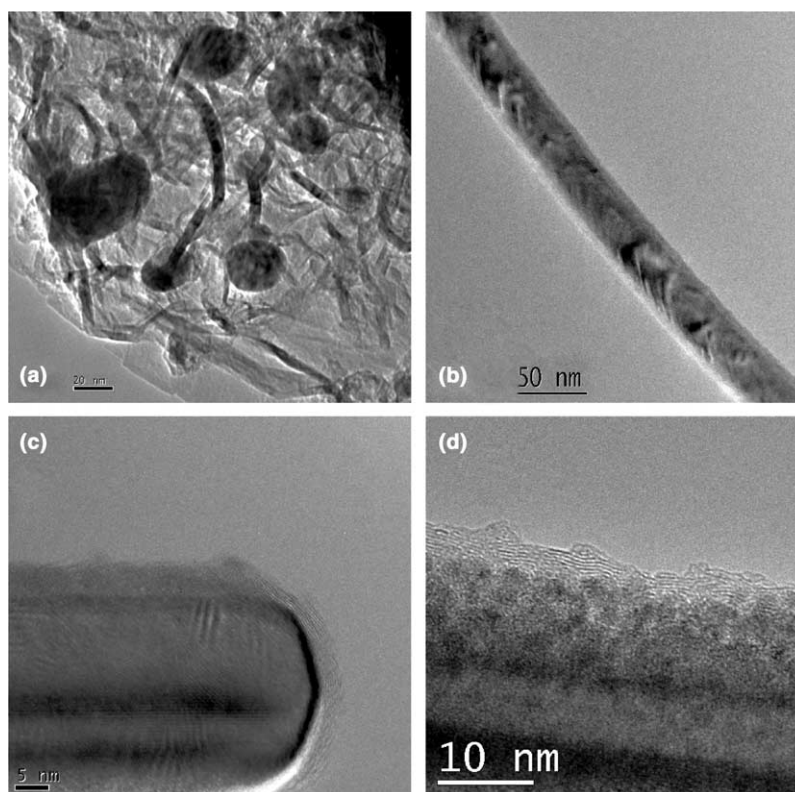


Fig. 4. TEM images showing: (a) metallic nanoparticles exhibiting capillary flow and being entrapped in the mass of BN sheets; (b) image of a long iron nanowire encapsulated in BN. Higher magnification images in (c) and (d) reveal that the interface between the BN and Fe consists of disordered *h*-BN.

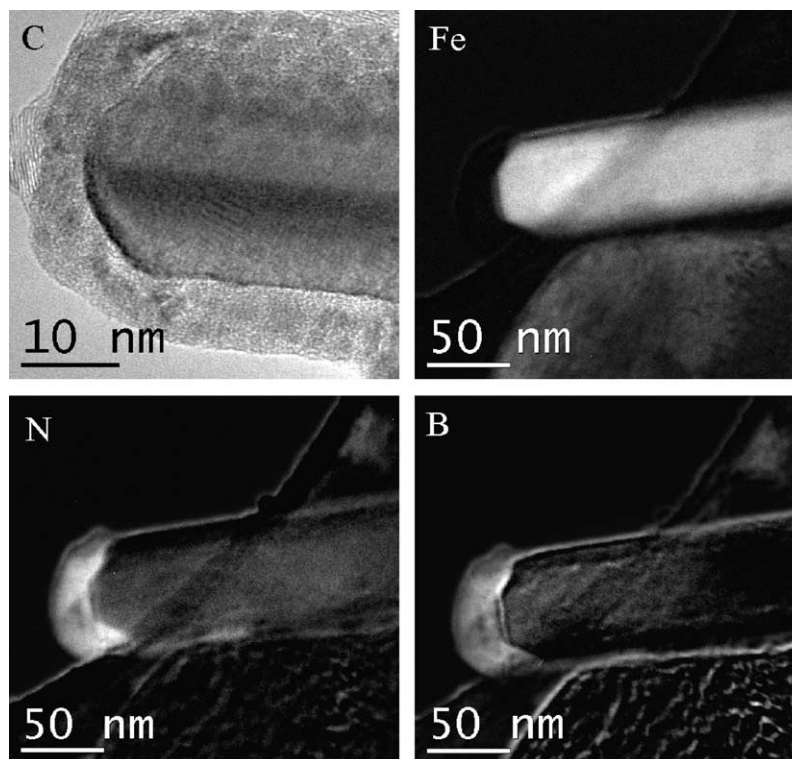


Fig. 5. Electron energy loss elemental mapping of BN ensheathed-Fe nanowire, showing individual elemental map of C, Fe, N and B, respectively. The area of bright contrast indicates the presence of the respective element. The results show that the core is filled with elemental iron, whilst the sheath is made of BN.

dered hexagonal BN by the ion beam sputtering of BN-Fe nanocomposite film [22]. They attributed the high shape anisotropy to the activated surface diffusion of the incoming deposited species assisted by ion beams. In the work described here, many BN lamina sheets, as well as small isolated FeB particles were left behind in an extended matrix after the encapsulated FeB particles escaped and coagulated into bigger particles. These lamina sheets may curl up to form BN nanotubes with the metal particle encapsulated within. Plasma-activated nitrogen and hydrogen species in our experiment may also impart energy for the activated diffusion of Fe on the dimensional BN lamina sheets, resulting in the anisotropic crystallization of metallic nanowires.

#### 4. Conclusions

We have demonstrated that the nitrogen plasma treatment of FeB nanoparticles at the eutectic melting point of the alloy can give rise to a range of BN nanomaterials, ranging from BN bamboo-like nanotubes, to nanotubules and microspheres, as well as iron nanowires encapsulated in BN. The mechanism of the phase segregation of BN from a dynamically flowing liquid FeB particle is interesting, because in its path, nanotubules, and nanospheres can be created by a shape

transform of its outline, similar to mold-casting. Our results suggest that capillary flow may provide a controlled way of creating dimensional nanostructures, i.e. by creating nanochannels on a substrate to facilitate the capillary flow of FeB to make BN nanotubes, or BN-ensheathed Fe nanowires.

#### Acknowledgements

The authors wish to acknowledge the financial support of NUS/SERC co-funded project entitled: 'Ion Beam Assisted Deposition of Boron Nitride Nanomaterials for Advanced Technological Applications' (Grant No: R-143-000-165-112/303).

#### References

- [1] X. Blasé, A. Rubio, S.G. Louie, M.L. Cohen, *Europhys. Lett.* 28 (1994) 335.
- [2] T. Laude, Y. Matsui, A. Marraud, B. Jouffrey, *Appl. Phys. Lett.* 76 (2000) 3239.
- [3] Renzhi Ma, Yoshio Bando, Tadao Sato, Keiji Kurashima, *Chem. Phys. Lett.* 350 (2001) 434.
- [4] John Cumings, A. Zettl, *Chem. Phys. Lett.* 316 (2000) 211.
- [5] B.G. Demczyk, J. Cumings, A. Zettl, R.O. Ritchie, *Appl. Phys. Lett.* 78 (2001) 2772.

- [6] R.S. Lee, J. Gavillet, M. Lamy de la Chapelle, A. Loiseau, J.-L. Cochon, D. Pigache, *Phys. Rev. B* 64 (2001) 121405.
- [7] Ying Chen, Lewis T. Chadderton, John Fitz Gerald, James S. Williams, *Appl. Phys. Lett.* 74 (1999) 2960.
- [8] A. Loiseau, F. Willaime, N. Demoncey, G. Hug, H. Pascard, *Phys. Rev. Lett.* 76 (1996) 4737.
- [9] D. Goldberg, Y. bando, M. Eremets, K. Takemura, K. Kurushima, H. Yusa, *Appl. Phys. Lett.* 69 (1996) 2045.
- [10] Oleg A. Louchev, *Appl. Phys. Lett.* 71 (1997) 3552.
- [11] I. Narita, T. Oku, *Diam. Relat. Mater.* 11 (2002) 949.
- [12] I. Narita, T. Oku, *Diam. Relat. Mater.* 12 (2003) 1146.
- [13] I. Narita, T. Oku, *Solid State Commun.* 122 (2002) 465.
- [14] D. Babonneau, M. Jaouen, M.-F. Denanot, P. Guérin, F. Petroff, *Appl. Phys. Lett.* 82 (2003) 3056.
- [15] Heng Zhang, Kian Ping Loh, *Diam. Related Mater.* 13 (2004), available on line 9 January 2004.
- [16] T. B. Massalski, J.L. Murray, L.H. Bennett, U. Baker (Eds.), *Binary Alloy Phase Diagrams*, American Society for Metals, Metals Park, OH, 1986.
- [17] Oleg A. Louchev, *J. Chem. Phys.* 118 (2002) 7622.
- [18] L.T. Chadderton, Ying Chen, *J. Cryst. Growth* 240 (2002) 164.
- [19] L.T. Chadderton, Y. Chen, *Phys. Lett. A* 263 (1999) 401.
- [20] S. Komatsu, Y. Shimizu, Y. Moriyoshi, K. Okada, M. Mitomo, *Appl. Phys. Lett.* 79 (2001) 188.
- [21] S. Komatsu, Y. Shimizu, Y. Moriyoshi, K. Okada, M. Mitomo, *J. Appl. Phys.* 91 (2002) 618.
- [22] D. Babonneau, M. Jaouen, M.-F. Denanot, P. Guérin, F. Petroff, *Appl. Phys. Lett.* 82 (2003) 3056.